PERGAMON

Solid State Communications 110 (1999) 381–386

solid state communications

Lattice vibrations in spin-Peierls compound NaV_2O_5

Z.V. Popović[a,*,†], M.J. Konstantinović[a], R. Gajić[a], V. Popov[b], Y.S. Raptis[c], A.N. Vasil'ev[d], M. Isobe[e], Y. Ueda[e]

[a]*Institute of Physics, 11001 Belgrade, P.O. Box 57, Yugoslavia*
[b]*Faculty of Physics, University of Sofia, 1126 Sofia, Bulgaria*
[c]*Physics Department, National Technical University, 15780 Athens, Greece*
[d]*Low Temperature Department, Moscow State University, 119899 Moscow, Russia*
[e]*Institute for Solid State Physics, The University of Tokyo, Roppongi 7-22-1, Minatoku, Tokyo 106, Japan*

Received 23 September 1998; accepted 10 February 1999 by D. Lockwood

Abstract

We present the room temperature far-infrared reflectivity and Raman scattering spectra of NaV_2O_5 single crystals. The frequencies of infrared active modes are obtained by an oscillator fitting procedure of reflectivity data. The assignment of the vibrational modes is given according to a lattice dynamical calculation based on the valence shell model. Besides phonon modes we observed broad features centered at about 280, 550 and 3500 cm^{-1} in infrared spectra for **E** ∥ **a** polarization and at about 640 cm^{-1} in Raman spectra for (aa) polarization. These structures are explained as crystal-field-splitting-induced d–d electronic transitions of V^{4+} ions. © 1999 Elsevier Science Ltd. All rights reserved.

Keywords: D. Phonons; E. Inelastic light scattering; E. Light absorption and reflection

It was shown recently [1] that sodium vanadium oxide is the second example of an inorganic spin-Peierls compound following $CuGeO_3$ [2]. The spin-Peierls transition results in spin dimerization due to coupling of the lattice phonons and spins [3]. Thus, the knowledge of phonon properties of crystals exhibiting the spin-Peierls instability, is necessary for a complete understanding of this effect.

The first determination of the NaV_2O_5 crystal structure [4] showed that this oxide has an orthorhombic unit cell with parameters $a = 1.1318$ nm, $b = 0.3611$ nm, $c = 0.4797$ nm, $Z = 2$ and the space group $P2_1mn$ (D_{2v}^7). Such a crystalline structure assumes two kinds of vanadium chains along the *b*-axis. One is magnetic V^{4+} ($S = 1/2$) and the other one is a nonmagnetic V^{5+} ($S = 0$) chain. Each vanadium atom is surrounded by five oxygen atoms, forming VO_5 pyramids. These pyramids are mutually connected via common edges to form a layers in (*ab*)-plane. The Na atoms are situated between these layers as intercalants. Most recently, the crystal structure of this oxide was reinvestigated [5]. It was shown that NaV_2O_5 crystallizes in centrosymmetric space group Pmmn (D_{2h}^{13}) with nearly the same unit cell parameters as previously stated [4], but with only one crystallographic vanadium position in mixed valence state (formal oxidation state is +4.5). A schematic representation of this crystal structure in (010)-plane is given in Fig. 1.

The previous polarized infrared transmission [6,7] and Raman scattering spectra [7,8] of NaV_2O_5 above

* Corresponding author.
† Present address: Laboratory of Solid State Physics and Magnetism, Department of Physics, University of Leuven, Celestijnenlaan 200D, B-3001 Leuven, Belgium.

PII: S0038-1098(99)00081-2

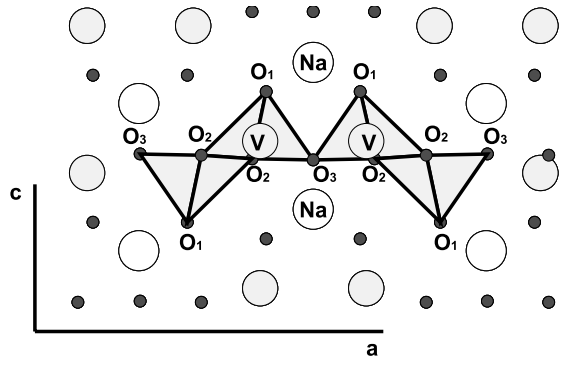

Fig. 1. Schematic representation of the NaV_2O_5 crystal structure in the (010) plane.

and below the spin-Peierls transition temperature reveal a crystallographic distortion at the transition temperature. No assignment of the observed modes was given. In our earlier paper [9] the polarized Raman and infrared spectra from the (001) plane are measured and the valence shell model lattice dynamical calculation was conducted taking into account the $P2_1mn$ space group symmetry of crystal structure of NaV_2O_5. It was shown that the space group of the NaV_2O_5 crystal structure cannot be $P2_1mn$ (non-centrosymmetric), but the space group which includes the mutual exclusion between Raman and infrared activity (centrosymmetric space group Pmmn).

Most recently [10,11], the temperature dependent optical conductivity of NaV_2O_5 was investigated. It was concluded that two-magnon optical absorption process takes place.

In this work we present polarized far-infrared (FIR) reflectivity as well as Raman scattering spectra of the single crystal NaV_2O_5 at room temperature for all principal polarizations. The $8A_g$, $5B_{2g}$, $3B_{3g}$, $7B_{3u}$, $4B_{2u}$ and $5B_{1u}$ symmetry modes are experimentally observed. The assignment of vibrational modes is given according to the lattice dynamical calculation based on valence shell model for Pmmn space group symmetry.

The present work was performed on single crystals, grown from the melt, using the self-flux method [12]. The crystals were plates with dimensions typically about $1 \times 4 \times 1\ mm^3$ in the a, b and c axes, respectively. The infrared measurements were carried out with a BOMEM DA-8 FIR spectrometer. A DTGS pyroelectric detector was used to cover the wave number region from 100 to 700 cm^{-1}; a liquid nitrogen cooled HgcdTe detector was used from 500 to 6000 cm^{-1}. Spectra were collected with 2 cm^{-1} resolution, with 500 interferometer scans added for each spectrum. The Raman spectra were measured in the backscattering configuration using micro-Raman system with Jobin Yvon 64000 triple monochromator including liquid nitrogen cooled CCD-detector. An Ar-ion laser was used as an excitation source.

The NaV_2O_5 unit cell consists of two formula units comprising 16 atoms in all. The site symmetries of Na, V, and O ions in Pmmn space group [5] are: C_{2v}(Na, O_3) and C_s(V, O_1, and O_2). The Factor-group-analysis (FGA) yields [9,13]:

V, O_1, O_2 (C_s): $\Gamma = 2\ A_g + A_u + B_{1g} + 2\ B_{1u} + 2\ B_{2g} + B_{2u} + B_{3g} + 2\ B_{3u}$

Na, O_3 (C_{2v}): $\Gamma = A_g + B_{1u} + B_{2g} + B_{2u} + B_{3g} + B_{3u}$

Summarizing these representation and subtracting acoustic ($B_{1u} + B_{2u} + B_{3u}$) and silent ($3A_u$) modes, we obtained the irreducible representations of NaV_2O_5 vibrational modes of Pmmn space group:

$$\Gamma = 8A_g(aa, bb, cc) + 3B_{1g}(ab) + 8B_{2g}(ac) + 5B_{3g}(bc) + 7B_{1u}(\mathbf{E} \parallel \mathbf{c}) + 4B_{2u}(\mathbf{E} \parallel \mathbf{b}) + 7B_{3u}(\mathbf{E} \parallel \mathbf{a})$$

Thus, 24 Raman and 18 infrared active modes are to be expected in the NaV_2O_5 spectra.

The room temperature far-infrared reflectivity spectra of NaV_2O_5 for all principal polarizations are given in Fig. 2. The open circles are the experimental data and the solid lines represent the spectra computed using a four-parameter model for the dielectric constant [14]. The best fit parameters are given in Table 1. The agreement between observed and calculated reflectivity spectra is rather good for $\mathbf{E} \parallel \mathbf{b}$ and $\mathbf{E} \parallel \mathbf{c}$ polarizations. For the $\mathbf{E} \parallel \mathbf{b}$ polarization, four oscillators with TO frequencies at about 178, 230, 370 and 582 cm^{-1} are clearly seen. In the high frequency region the measured reflectivity shows a small dip (relative to the calculated curve) near 620 cm^{-1}. We believe that this dip arises from an $\mathbf{E} \parallel \mathbf{a}$ LO mode as a consequence of the deviation of normal incidence. As a support for this interpretation we found well defined 620 cm^{-1} reflectivity edge in our non-polarized reflectivity spectra from the (001) plane.

In the $\mathbf{E} \parallel \mathbf{c}$ polarization (Fig. 2(c)) four oscillators at 164, 181, 460 and 955 cm^{-1} are clearly seen. The

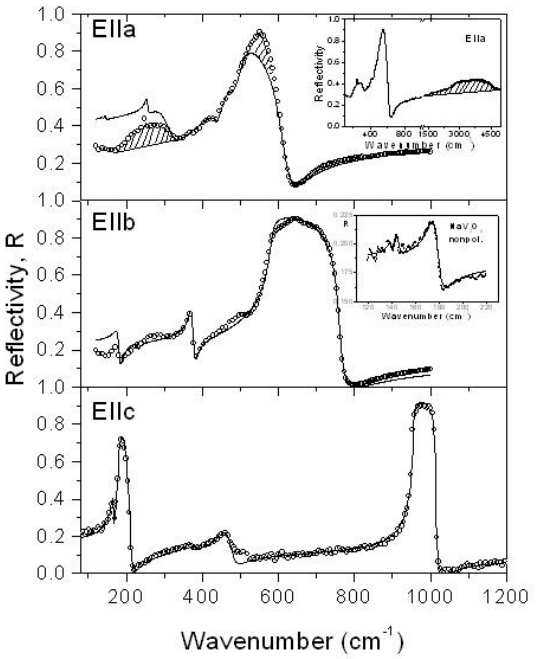

Fig. 2. Room temperature polarized far-infrared reflectivity spectra of NaV_2O_5 single crystal for the **E** ∥ **a** (a), **E** ∥ **b** (b) and **E** ∥ **c** (c) polarizations. The experimental values are given by open circles. The solid lines represent the calculated spectra obtained by a fitting procedure described in text. The inset of (a): The **E** ∥ **a** polarized reflectivity spectra in the wide spectral range up to 6000 cm^{-1}. The inset of (b): Non-polarized reflectivity spectra in the 120–220 cm^{-1} spectral range.

oscillator at 368 cm^{-1} is probably a leakage of the 370 cm^{-1} phonon from the **E** ∥ **b** polarization. The disagreement between calculated and experimental data at around 500 cm^{-1} comes from a beam-splitter change.

In the **E** ∥ **a** polarization disagreement between calculated and measured spectra arises due to presence of the continuum features centered at about 280 and 550 cm^{-1}. One broad structure centered at 3500 cm^{-1} is also observed in this polarization, right inset in Fig. 2(a). While the 280 cm^{-1} continuum is clearly seen, the presence of the 550 cm^{-1} continuum is manifested through quite uncharacteristic oscillator shape of dominant structure between 500 and 620 cm^{-1}. Similar continuum is observed in room temperature Raman spectra and we will discuss it latter on. Besides these continua (denoted by ''shadow regions'' in Fig. 2(a)) seven oscillators with TO energies at 138, 144.5, 254, 438, 469, 505 and 939.8 cm^{-1} are observed. Due to the low signal intensity from small samples for polarized light, the energies of the lowest frequency modes are obtained by a fitting procedure of non-polarized reflectivity spectrum. The presence of the lowest frequency modes merely disrupts the interference fringes in the spectral range depicted in the right inset of Fig. 2(b).

Table 1
Oscillator fit parameters in cm^{-1}

Polarization	ω_{TO}	γ_{TO}	ω_{LO}	γ_{LO}	ε_∞
	138	5.8	138.2	5.8	
	144.5	4.5	144.7	5	
	254	9	256	10	
	(290)	(80)	(232)	(50)	
E ∥ **a**	438	30	439	21	4.3
	469	22	473	27	
	505	25	624	45	
	939.8	7.5	940	8.5	
	(3400)	(1700)	(5500)	(6000)	
	178	15	183	9	
E ∥ **b**	230.5	5	231	4.5	4.5
	370	12	378	10	
	582	12	762	15	
	164	5	166	4	
	181	6	212	10	
E ∥ **c**	368	25	370	30	3.5
	460	35	480	35	
	955	4	1014	3	

The room temperature Raman spectra of NaV_2O_5, for parallel and crossed polarizations, are given in Fig. 3. The spectra for parallel polarizations consist of A_g symmetry modes. Seven modes at 90, 179, 305, 420, 448, 534 and 969 cm^{-1} are clearly seen for the (aa) polarization and one additional mode at 233 cm^{-1} for the (bb) polarization. The mode at 423 cm^{-1} is highest intensity mode for (bb) polarization. Its counterpart appears in (aa) polarization at 420 cm^{-1}. The frequency shift of this mode in (aa) polarization is due to interaction of 448 cm^{-1} mode with electronic background peaked at 640 cm^{-1}. For the crossed (ab) polarization three Raman active B_{1g} symmetry modes at 175, 294 and 683 cm^{-1} are observed. In the case of the (ac) polarization, five B_{2g} symmetry modes at 149, 192, 226, 550 and 954 cm^{-1} were observed. Because of low-quality of the (010) surface, this spectrum contains also the modes from other polarizations. Finally, the B_{3g} symmetry modes at 260, 366 and 684 cm^{-1} were observed for the (bc) polarization configuration.

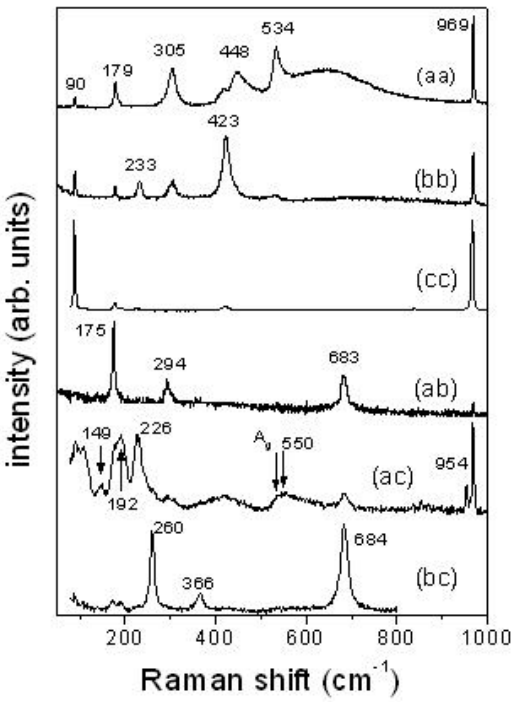

Fig. 3. Raman scattering spectra at room temperature for different polarization configurations. Laser excitation line was 488 nm.

The frequencies of all observed IR and Raman active modes, together with previously published results, are collected in Table 3. Besides general agreement between these data, there are some exceptions. Namely, four B_{1g} modes are observed in Ref. [8], one mode more than the FGA predicts. We believe that the mode at 262 cm^{-1} [8] is B_{3g} symmetry mode since we found the mode at 260 cm^{-1} in our spectra with the B_{3g} symmetry configuration. The frequencies of the other three B_{1g} modes from Ref. [8] agree well with our data for the same symmetry configuration. From comparison between our data and those from Ref. [7] we found that the resolution and signal-to-noise ratio of our spectra are much better than in [7]. Thus, only the strongest intensity modes from [7] agree with our spectra. The other low intensity modes of A_g symmetry observed [7] at about 215, 254, 415, 435 cm^{-1} are probable noise. In the case of the crossed polarizations, the spectra from [7] show a mixture of B and A_g symmetry modes. For (ab) polarization, the spectrum of Smirnov et al. [7], corresponds to our spectrum, while for (ac) polarization

Table 2
Valence shell model parameters for NaV_2O_5.

VSM parameter		Value
bond-stretching force constant (mdyn/Å)	$V - O_1$	17.90
	$V - O_{2,3}$	2.21
angle-bending force constant (mdyn.Å/rad^2)	$V - O_2 - V$	0.98
	$O_1 - V - O_2$	-0.15
	$O_1 - V - O_3$	0.77
	$O_2 - V - O_2$	-1.89
	$O_2 - V - O_3$	1.02
	$O_{2,3} - V - O^*_{2,3}$	0.84
ionic charge (| *e* |)	Na	0.11
	V	1.84
	O	-0.76
shell charge (| *e* |)	Na	3.31
	V	2.55
	O	-2.43
ionic polarizability (Å^3)	Na	0.75
	V	1.78
	O	1.95

only two modes at 190 and 224 are with B_{2g} symmetry. All other modes for this symmetry configuration at 89, 176, 308, 531 and 970 cm^{-1} [7] are actually the A_g modes. In the case of (bc) polarization three modes at 260, 365 and 685 cm^{-1} are with B_{3g} symmetry, while two other modes of this configuration at 89 and 970 cm^{-1} represent a ''leakage'' from A_g symmetry configuration. In the case of infrared mode frequencies there is a rather good agreement between previously published and our data for almost all modes except for the mode at about 500 cm^{-1}. We have shown that this mode is a superposition of one oscillator and continuum peaked at about 550 cm^{-1}. Finally, there is a minor frequency difference for some Raman modes between our previously published paper [9] and the present one. These corrections come from more precise calibration.

The calculation of the Γ-phonons of NaV_2O_5 was carried out within a valence shell model (VSM). Details on the valence shell model and the types of model parameters are given in Ref. [15]. Apart from the valence force fields of bond-stretching and angle-bending types, a Born-type repulsion potential was used for the sodium–oxygen interactions and a weak Van der Waals attraction was accepted for the oxygen–oxygen interactions. Born-type repulsion parameters were: a = 800 eV; b = 3.52 Å^{-1}; and

Table 3
Calculated frequencies of the Γ phonons in NaV_2O_5

Mode	Ref. [7]	Ref. [8]	Ref. [9]	Ref. [10]	Ref. [11]	This work	calc.	Remark
	89	88	90	-	-	90	102	chain rotation
	175	178	179	-	-	179	159	Na ‖ **c**
	231	-	234	-	-	233	227	O-V-O bending
A_g	300	304	306	-	-	305	298	O-V-O bending
	421	420	424	-	-	423	385	O-V-O bending
	449	-	452	-	-	448	466	$V\text{-}O_3\text{-}V$ bending
	531	530	536	-	-	534	501	$V\text{-}O_2$ stretching
	970	970	969	-	-	969	949	$V\text{-}O_1$ stretching
	172	173	175	-	-	175	182	chain rotation
B_{1g}	289	292	297	-	-	294	293	O-V-O bending
	678	685	684	-	-	683	685	$V\text{-}O_2$ stretching
	-	-	-	-	-	149	143	Na ‖ **a**
	190	-	-	-	-	192	170	chain rotation
	224	-	-	-	-	226	223	O-V-O bending
B_{2g}	308	-	-	-	-	-	277	O-V-O bending
	-	-	-	-	-	-	383	O-V-O bending
	-	-	-	-	-	-	497	$V\text{-}O_2$ stretching
	-	-	-	-	-	550	535	$V\text{-}O_3$ stretching
	-	-	-	-	-	954	966	$V\text{-}O_1$ stretching
	-	-	-	-	-	-	128	chain rotation
	-	-	-	-	-	-	232	Na ‖ **b**
B_{3g}	260	262	-	-	-	260	274	O-V-O bending
	365	-	-	-	-	366	373	$V\text{-}O_3\text{-}V$ bending
	685	-	-	-	-	684	680	$V\text{-}O_2$ stretching
						silent	138	chain transl. ‖ **b**
A_u						silent	204	O-V-O bending
						silent	569	$V\text{-}O_2$ stretching
	-	-	-	-	-	164/166	160/160	chain rotation
	-	-	-	-	-	181/212	174/175	Na ‖ **c**
	-	-	-	-	-	-	277/277	O-V-O bending
B_{1u}	-	-	-	-	-	(368/370)	375/375	O-V-O bending
	-	-	-	-	-	460/480	478/478	$V\text{-}O_3\text{-}V$ bending
	-	-	-	-	-	-	488/488	$V\text{-}O_2$ stretching
	-	-	-	-	-	955/1014	945/945	$V\text{-}O_1$ stretching
	175	-	177	175	177	178/183	167/177	O-V-O bending + Na ‖ **b**
B_{2u}	-	-	-	229	225	230.5/231	232/260	Na ‖ **b**
	367	-	372	367	371	370/378	374/376	$V\text{-}O_3\text{-}V$ bending
	587	-	582	581	586	582/762	568/764	$V\text{-}O_2$ stretching
	-	-	140	-	137	138/138.2	135/137	chain transl. ‖ **c**
	145	-	-	145	-	144.5/144.7	158/158	Na ‖ **a**
	251	-	254	251	256	254/256	252/264	O-V-O bending
B_{3u}	-	-	436	-	-	438/439	405/405	O-V-O bending
	-	-	469	-	-	469/473	486/486	$V\text{-}O_2$ stretching
	526	-	505	524	518	505/624	534/536	$V\text{-}O_3$ stretching
	-	-	940	-	938	939.8/940	953/960	$V\text{-}O_1$ stretching

O–O interaction potential was taken from Ref. [16]. The initial values of the model parameters were taken from a lattice-dynamical study of V_2O_5 for which infrared and Raman data exist [17]. The final model parameter values, given in Table 2, are obtained from comparison between measured and calculated phonon frequencies for NaV_2O_5.

The phonon frequencies for NaV_2O_5 calculated

with the best fit model parameters are shown in comparison to the observed lines in the Raman and the infrared spectra in Table 3. There is an overall good agreement with the experimental data with largest deviations not exceeding 10%.

There are several modes associate with large displacements of sodium atoms. For the modes of A_g and B_{1u} symmetry class, calculated to be at 159 and 174 cm^{-1}, the Na atoms move mainly along the *c*-axis, while for the modes of B_{3g} and B_{2u} symmetry (232 and 232/260 cm^{-1}) the Na atoms move along the *b*-axis. Finally, there are two modes with B_{2g} (170 cm^{-1}) and B_{3u} (158 cm^{-1}) symmetry for which the displacements of Na atoms are predominantly along the *a*-axis. The measured Raman and infrared spectra allow assignation of the peak at 179 cm^{-1} (181 cm^{-1}) to the mentioned A_g (B_1u) modes.

According to the Table 3 the modes in the spectral range between 200 and 500 cm^{-1} are bond bending vibrations, while the higher frequency modes originate from stretching vibrations of V–O atoms. The shorter V–O distance gives the higher mode frequency. Thus, the highest frequency modes at 969 cm^{-1} (Raman) and 940 cm^{-1} (IR) represent $V–O_1$ stretching vibrations, the modes at about 600 cm^{-1} originate from $V–O_2$ stretching vibrations. Note that the Raman mode at 448 cm^{-1}, which originates from $V–O_3–V$ bending vibrations, could be sensitive to Na deficiency since Na vacancy produce the change of bending angle.

The full assignment of all optical modes is given in Table 3 and we do not repeat it here in detail.

We suggest that all non-phononic modes in IR (at 280, 550 and 3500 cm^{-1}) and Raman spectra (at 640 cm^{-1}) originate from electronic transitions between d–d levels of V^{4+} ions. According to simplified scheme given in [7,18], which considers 3d orbital state in the VO_5 pyramid, there are five electronic levels by crystal field of c_s symmetry. The lowest level could be at 280 cm^{-1}, and the next levels at about 600 cm^{-1}, 3500 cm^{-1}, and 1.25 eV [7].

In conclusion, we presented far infrared and Raman spectra of NaV_2O_5 single crystal. FGA predicts 24 Raman and 18 IR active modes. We experimentally observed 19 Raman and 16 IR modes which represent the most complete list, up to now. The mode assignment is given according to shell model lattice dynamical calculation. This calculation was conducted, for the first time, taking into account the new crystal symmetry determination of this compound (Pmmn space group). We found a very good agreement between the experimental data and calculated frequencies. We believe that all non-phononic modes in IR and Raman spectra originate from electronic transitions between d–d levels of V^{4+} ions.

Acknowledgements

This work was supported by Serbian Ministry of Science and Technology under Project 01E09 and by National Technical University of Athens.

References

[1] M. Isobe, Y. Ueda, J. Phys. Soc. Japan, 65 (1996) 1178.
[2] M. Hase, I. Terasaki, K. Uchinokura, Phys. Rev. Lett., 70 (1993) 3651.
[3] E. Pytte, Phys. Rev. B 10 (1974) 4637.
[4] A. carpy, J. Galy, Acta crystallogr. B 31 (1975) 1481.
[5] H.G. von Schnering, Yu. Grin, M. Kaupp, M. Somer, R.K. Kremer, O. Jepsen, T. chatterji, M. Weiden, Z. Kristallogr., 213 (1998) 246.
[6] M.N. Popova, A.B. Sushkov, A.N. Vasil'ev, M. Isobe, Y. Ueda, Pis'ma Zh. Eksp. Teor. Fiz. 65 (1977) 711.[Engl. transl. JETP Lett. 65 (1997) 743.]
[7] S.A. Golubchik, M. Isobe, A.N. Ivlev, B.N. Mavrin, M.N. Popova, A.B. Sushkov, Y. Ueda, A.N. Vasil'ev., J. Phys. Soc. Japan, 66 (1997) 4042.
[8] M. Weiden, R. Hauptmann, c. Geibel, F. Steglich, M. Fischer, P. Lemmens, G. Guntherodt, Z. Phys. B 103 (1997) 1.
[9] Z.V. Popović, M.J. Konstantinović, R. Gajić, V. Popov, Y.S. Raptis, A.N. Vasil'ev, M. Isobe, Y Ueda, J. Phys.: condensed Mater, 10 (1998) L513.
[10] D. Smirnov, P. Millet, J. Leontin, D. Poilblanc, J. Riera, D. Augier, P. Hansen, Phys. Rev. B 57 (1998) R11035.
[11] A. Damascelli, D. van der Marel, M. Grüninger, c. Presura, T.T.M. Palstra, J. Jegondez, A. Revcolevschi, Phys. Rev. Lett. 81 (1998) 918.
[12] M. Isobe, c. Kagami, Y. Ueda, J. crystal Growth, 181 (1997) 314.
[13] D.L. Rousseau, R.P. Bauman, S.P.S. Porto, J. Raman Spectrosc., 10 (1981) 253.
[14] Z.V. Popović, S.D. Dević, V.N. Popov, G. Dahlenne, A. Revcolevschi, Phys. Rev. B 52 (1995) 4185.
[15] K. Kunc, H. Bilz, Solid State Commun., 19 (1976) 1027.
[16] C.R.A. catlow, W.C. Mackrodt, M.J. Norgett, A.M. Stoneham, Phys. Mag., 35 (1977) 177.
[17] P. clauws, J. Broeckx, J. Vennik, Phys. Stat. Sol. (b), 131 (1985) 459.
[18] T. Ohama, H. Yasuoka, M. Isobe, Y. Ueda, J. Phys. Soc. Japan, 66 (1997) 3008.